Journal of Power Sources, *32* (1990) 341 - 351

DEVELOPMENTAL STUDIES ON POROUS IRON ELECTRODES FOR THE NICKEL–IRON CELL

N. JAYALAKSHMI and V. S. MURALIDHARAN

Central Electrochemical Research Institute, Karaikudi 623 006 (India)

(Received June 30, 1989; in revised form April 9, 1990)

Summary

The development of sintered iron electrodes for the Ni–Fe battery is mainly aimed at increasing the discharge capacity and minimising self-discharge. Electrodes were prepared by either introducing additives into the iron powder before sintering or adding to powder before pressing. To evaluate the self-discharge characteristics, electrochemically-impregnated additives were studied by chronopotentiometry to determine the discharge behaviour and open-circuit-potential recovery transients of iron electrodes in the Ni–Fe cell. Mercury and sulphur benefit the iron electrode by increasing the discharge capacity and retarding the formation of FeOOH.

Introduction

Developmental studies on porous iron electrodes have received attention in recent years because of their use in Ni–Fe and Fe–air cells. Attention has focussed on improving charging efficiency and discharge capacity, and minimising self-discharge. Electrodes were prepared by either mixing additives before sintering or depositing them from the electrolyte to achieve the above goals [1 - 9]. Open-circuit potential recovery transients have been used to screen additives for suppressing self-discharge [10]. In this study, additives were incorporated into the porous iron electrodes by electrochemical impregnation and their performances were analysed using chronopotentiometry and the open-circuit potential recovery transients of assembled Ni–Fe cells.

Experimental

Preparation of iron electrodes

Electrolytic iron powder (α-Fe) of composition 99.1wt.%Fe, 0.01wt.%-Pb, 0.008wt.%Zn, 0.001wt.%As, 0.025wt.%Mn and 0.005wt.%Cu, and −300 mesh particle size was spread uniformly in a graphite die over

0378-7753/90/$3.50

a 10 mesh nickel grid of 0.1 mm thickness. The electrodes were sintered in the temperature range 970 - 1170 K for 60 min under a hydrogen atmosphere. The area and thickness of the electrode was 1.6 cm^2 and 2 mm, respectively. A copper rod was welded onto the pellet to provide electrical connection.

Iron electrodes of porosity 62.1% were cathodically impregnated with other metals using 0.1 M solutions of lead acetate, or mercury, silver, and copper nitrates. Sulphur was impregnated from 6.0 M KOH containing elemental sulphur. The impregnation was carried out by applying a cathodic current of 10 mA using a constant-current generator for 10 min.

Preparation of nickel electrodes

Loose, sintered nickel electrodes were prepared from INCO Nickel 255 powder previously reduced at 1175 K under a hydrogen atmosphere for 30 min. The powder was spread uniformly in a graphite die over a 10 mesh nickel grid of 0.1 mm thickness. The area and thickness of the electrode was 1.6 cm^2 and 2 mm, respectively.

Cell cathodes consisted of sintered nickel electrodes of porosity 70 - 80% and nickel sheets of purity 99.5% and size 5 × 1 cm were used as anodes. Impregnation was carried out using two anodes one on either side of the cathode at the rate of 20 mA for 90 min in an electrolytic bath of composition 3 M $Ni(NO_3)_2$, 0.25 M $Co(NO_3)_2$, 0.1 M $Cd(NO_3)_2$ and 0.1 M $MnSO_4$. The bath was maintained at pH 1 - 2 by adding formic acid [11].

Chronopotentiometric studies

A simple half-cell consisting of iron as working electrode, platinum foil as counter electrode, and an Hg/HgO reference electrode was used. The electrolyte was 6 M KOH containing 0.63 M LiOH. The iron electrode was subjected to a cathodic current of 90 mA for 30 min using a constant-current generator. After 30 min different anodic current steps in the range 15 - 60 mA were applied to the iron electrode. The cathodic polarisation was carried out on each occasion using the same current and after the application of each anodic current step, the variation of potential with time was followed using a printout voltmeter.

Open-circuit potential recovery studies

A 40 mA h cell was assembled with a single iron electrode and a single, higher-capacity nickel electrode using the same electrolyte as above. The cell was subjected to charge and discharge treatment at the $C/4$ rate for 10 cycles. The electrode capacity was then stabilised prior to recording the open circuit potential transients at different states of charge (SOC). The cell was charged at the same rate and discharged at different rates to obtain the required SOCs. The discharge circuit was then opened and the open-circuit potential of the iron electrode was followed (*versus* Hg/HgO) with time using the printout voltmeter.

Results and discussion

Chronopotentiometric studies

A basic assumption is made that all the applied anodic currents initiate the reaction between the electrode and the hydroxyl ions, and the mass transfer is controlled by the diffusion of the hydroxyl ions in solution. Figure 1 presents typical chronopotentiograms for a porous iron electrode at different applied anodic currents. At lower currents, the E–t curves indicated a gradual fall in potential while with increase in current a steep fall was observed. The initial fall is due to the partial oxidation of the iron surface along the charging electrical double layer. A constant potential region over a long transient time (τ_1) may be due to the formation of $Fe(OH)_2$ with thickening of the oxide film. It was proposed earlier [12] that the following reaction scheme is in operation:

$$Fe + OH^- \rightleftharpoons FeOH_{ad} + e^- \quad (1)$$

$$FeOH_{ad} \longrightarrow FeOH^+ + e^- \quad (2)$$

$$FeOH_{ad}^+ + OH^- \rightleftharpoons Fe(OH)_2 \quad (3)$$

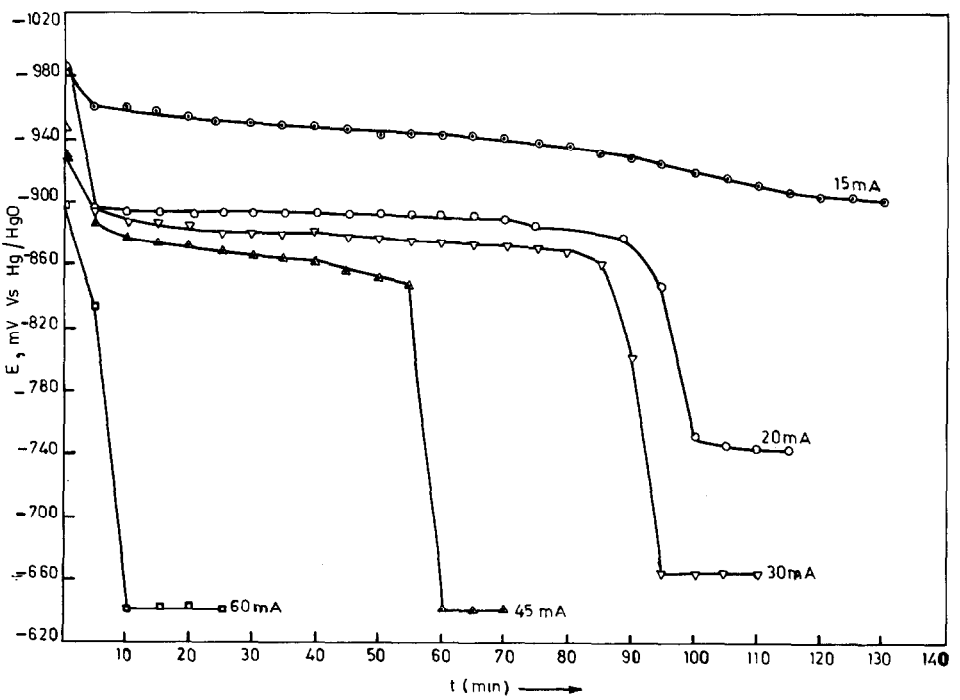

Fig. 1. Typical chronopotentiograms for a porous iron electrode at different anodic currents. ⊙, 15 mA; ○, 20 mA; ▽, 30 mA; △, 45 mA; □, 60 mA.

At the end of the first plateau, the change in potential is due to the further oxidation of $Fe(OH)_2$, and the appearance of the second plateau is due to the complete conversion of $Fe(OH)_2$ to FeOOH. At higher anodic potentials $Fe(OH)_2$ can react with OH^- to form FeOOH:

$$Fe(OH)_2 + OH^- \longrightarrow FeOOH + H_2O + e^- \quad (4)$$

The direct oxidation of Fe to FeOOH may also follow the same sequence. FeOOH can dissolve in 6.0 M KOH solution to yield Fe(III) species or $HFeO_2^-$.

Analysis of first plateau

Experiments were carried out with porous iron electrodes with incorporated additives. Table 1 presents the parameters derived from the first plateau of the chronopotentiograms. In general, in the presence of additives it was seen that increases in anodic currents shifted the formation potential of $Fe(OH)_2$ to more active iron values. At higher currents, most additives caused this electrode potential to become more negative than that for pure iron at the same current level; however, at 15 mA the $Fe(OH)_2$ formation potential became more noble. When compared with pure iron, additives mostly increased transient times.

To use iron as a battery electrode, knowledge of the ratio of the quantity of electricity consumed in the formation of iron hydroxide to the total charge passed will be helpful in evaluating the role of additives in increasing the discharge capacity.

$$\% \text{ utilisation} = \frac{Q_{\text{consumed}}}{Q_{\text{applied}}} \times 100 \quad (5)$$

where Q_{consumed} corresponds solely to the formation of $Fe(OH)_2$. For all anodic currents applied, the percentage of utilisation is increased in the presence of additives (Table 2).

The macrohomogeneous model of a porous electrode [13] assumes the whole electrode electrolyte as two continua and, in constant current electrolysis, for a planar electrode, the potential is given by the following equation for an irreversible wave [14]

$$E = E_e + \frac{RT}{\alpha_a F} \ln\left(\frac{i_0}{i}\right) + \frac{RT}{\alpha_a F} \ln\{1 - (t/\tau)^{1/2}\} \quad (6)$$

where E_e is the equilibrium potential and α_a is the anodic transfer coefficient.

A plot of E *versus* $\ln\{(\sqrt{\tau} - \sqrt{t})/\sqrt{\tau}\}$ is predicted to be linear for a given current with a slope of $(RT/\alpha_a F)$. Figure 2 is a plot of E *versus* $\ln(\sqrt{\tau} - \sqrt{t}/\sqrt{\tau})$ at 15 mA for iron electrodes containing additives. The parameters derived from E *versus* $\ln\{(\sqrt{\tau} - \sqrt{t})/\sqrt{\tau}\}$ for various applied currents are given in Table 3. It may be seen that a Tafel slope of approximately 60 mA was observed for iron, suggesting that a chemical step

TABLE 1

Parameters derived from first plateau of chronopotentiograms

System	15 mA		20 mA		30 mA		45 mA		60 mA	
	E_1 (mV)	τ_1 (min)	E_1 (mV)	τ_1 (min)	E_1 (mV)	τ_1 (min)	E_1 (mV)	τ_1 (min)	E_1 (mV)	τ_1 (min)
Fe	−950	90	−890	70	−870	70	−870	50	—	—
Fe + 0.82wt.%Hg	−915	110	−915	110	−900	110	−875	110	—	—
Fe + 10.9wt.%S	−900	110	−895	110	−880	110	−860	90	−845	50
Fe + 1.8wt.%Ag	−930	110	−920	110	−915	110	−910	60	−870	15
Fe + 1.17wt.%Pb	−900	110	−880	110	−870	55	—	—	—	—

TABLE 2

Percentage utilization of active material

System	15 mA		20 mA		30 mA		45 mA	
	$Q_{ap} = 30 \times 10^{-3}$ A h		$Q_{ap} = 40 \times 10^{-3}$ A h		$Q_{ap} = 60 \times 10^{-3}$ A h		$Q_{ap} = 90 \times 10^{-3}$ A h	
	Q_{con}	%	Q_{con}	%	Q_{con}	%	Q_{con}	%
Fe	22.5	75	22.3	58.3	25	41.6	37.5	41.6
Fe + 0.82wt.%Hg	27.5	91.6	36.6	91.6	55	91.6	82.5	91.6
Fe + 10.9wt.%S	27.5	91.6	36.6	91.6	55	91.6	67.5	75
Fe + 1.8wt.%Ag	27.5	91.6	36.6	91.6	55	91.6	45	50
Fe + 1.17wt.%Pb	27.5	91.6	36.6	91.6	27.5	45.8	—	—

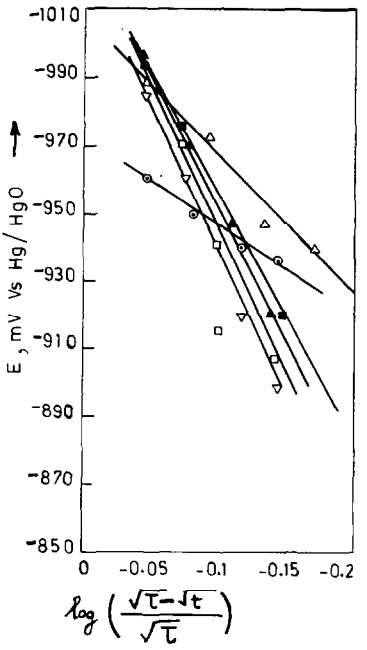

Fig. 2. E *vs.* $\ln\{\sqrt{\tau} - \sqrt{t}/\sqrt{\tau}\}$ plot for iron electrodes with additives. ⊙, Fe; △, Fe + Ag; ▲, Fe + S; □, Fe + Pb; ■, Fe + Hg; ▽, Fe + Cu.

TABLE 3

Parameters obtained from E *vs.* $\ln\{\sqrt{\tau} - \sqrt{t}/\sqrt{\tau}\}$ plot

System	Anodic Tafel slope (±0.5 mV/decade)		
	15 mA	20 mA	30 mA
Fe	53	66	60
Fe + 0.82 wt.%Hg	40	40	40
Fe + 10.9wt.%S	150	150	150
Fe + 1.8wt.%Ag	53	56	60
Fe + 1.17wt.%Pb	135	135	85

following eqn. (1) may be a slow step, or the adsorption of OH^- ion may follow isotherms other than Langmuir.

Additions of sulphur and lead increase the Tafel slope while mercury has the opposite effect. Caution should be exercised in interpreting the significance of the Tafel slope, as the presence of additives would have altered the surface area of the iron electrode and the effective current density. It has been observed earlier that for a planar electrode the value of the product $i\sqrt{t}$ is constant over a time interval of seconds [15, 16] in aqueous solutions and in molten media, obeying Sand's equation [17] which assumes that the rate of reaction depends on the speed of diffusion

TABLE 4

Values of $i\sqrt{\tau}$ for different anodic currents

System	15 mA	20 mA	30 mA	45 mA
Fe	142.3	167.3	250.9	318.2
Fe + 0.82wt.%Hg	157.3	209.7	314.6	471.9
Fe + 10.9wt.%S	157.3	209.8	314.6	426.0
Fe + 1.8wt.%Ag	157.3	209.8	314.6	348.6
Fe + 1.17wt.%Pb	157.3	209.8	222.5	—

of electro-active species. In the case of porous, iron electrodes $it^{1/2}$ is not constant (Table 4) over the entire range of applied anodic current. Several factors may contribute to this discrepancy: the concentration gradient between the pores and the bulk of the electrolyte, edge diffusion–convection, and the contribution from the charging current. It was also observed that ir was variable for porous iron electrodes in thin layer cells [18].

Analysis of second plateau

With continued passage of anodic current of 20 mA or more, a second plateau was observed (Fig. 1) at a potential at which the partial oxidation of $Fe(OH)_2$ to FeOOH takes place. From a battery point of view, the appearance of this second plateau due to the formation of FeOOH is not advantageous. There is a significant drop in potential (−850 to −650 mV *versus* Hg/HgO) and recharging of this electrode would require higher charging currents. The performance of the electrode would be adversely affected with increase in the life cycle.

Mercury additions suppress the formation of FeOOH at all anodic currents, while sulphur, silver and lead delay the formation of FeOOH (Fig. 3) below 45 mA, with a shift to more negative plateau potentials (Table 5). Subsequently, these additives promote the recharging ability of the iron electrode.

Open-circuit potential recovery curves

Figure 4 presents the open circuit potential recovery transients for a porous iron electrode at various states of charge. It can be seen that the approach to equilibrium becomes increasingly sluggish as the SOC of the electrode is decreased. This is because the surfaces of the grains of electrode material are enriched with discharge products, while active-iron remains within the pores. The diffusion of hydroxyl ions into the interior sites of the pores varies when the state of charge is higher.

The potential–time transients at various SOC were obtained in the presence of additives, and Table 6 presents the corrosion potentials at different SOCs. The corrosion potentials lie between the equilibrium potentials of Fe/Fe(II) (−1.03 V) and Fe(II)/Fe(III) (−0.715 V *versus* Hg/HgO).

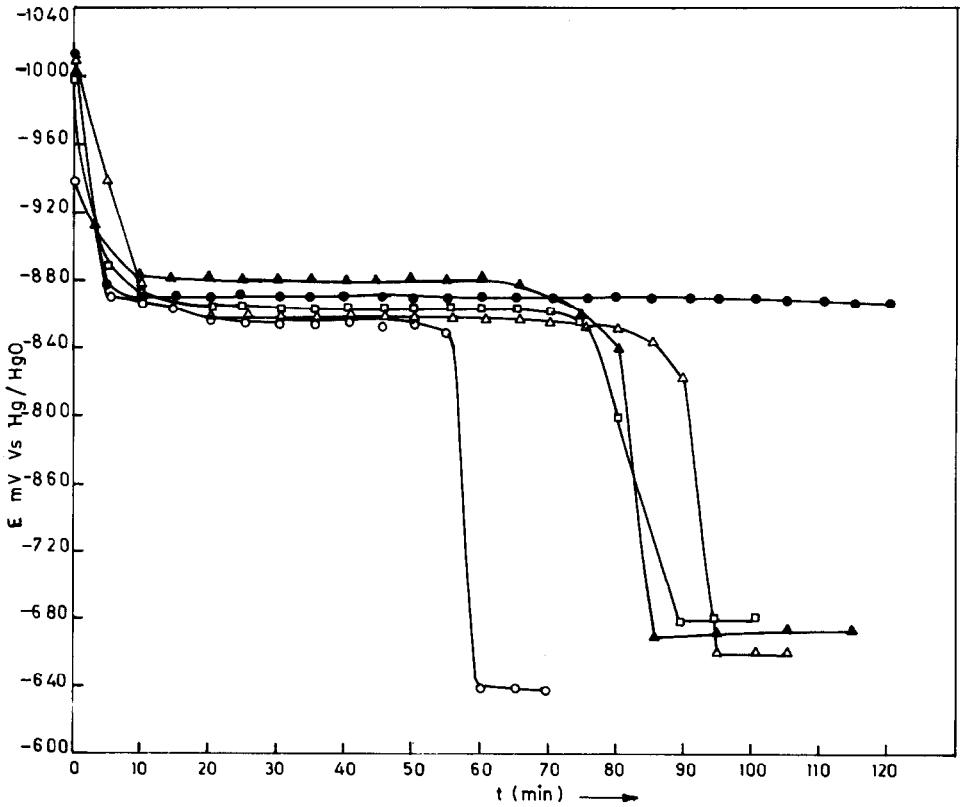

Fig. 3. Chronopotentiograms for iron electrodes with additives at an anodic current of 45 mA. ⊙, Fe; ●, Fe + Hg; △, Fe + S; □, Fe + Pb; ▲, Fe + Ag.

TABLE 5

Parameters derived from second plateau of chronopotentiograms

System	20 mA		30 mA		45 mA		60 mA	
	E_2 (mV)	τ_2 (min)	E_2 (mV)	τ_2 (min)	E_2 (mV)	τ_2 (min)	E_2 (mV)	τ_2 (min)
Fe	−740	15	−660	20	−640	10	—	—
Fe + 10.9wt.%S	—	—	—	—	−665	10	−650	5
Fe + 1.8wt.%Ag	—	—	—	—	−680	30	−660	15
Fe + 1.17wt.%Pb	—	—	−680	5	−610	10	—	—

Figure 5 presents the equilibrium potentials, E_e, of Fe/Fe(II) and Fe(II)/Fe(III) couples, and E_M the mixed potential or corrosion potential. There is no marked change in corrosion potential with state of charge, but there is in the presence of foreign ions. Additions of silver, copper and lead shift the potential in a more noble direction, while mercury and sulphur

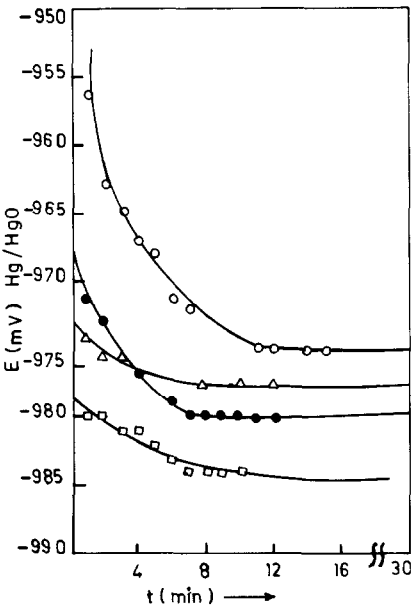

Fig. 4. Open-circuit-potential recovery transients for the iron electrode at different states of charge. ○, 97.5%; △, 98%; ●, 90%; □, 85%.

TABLE 6

Corrosion potential (*vs.* Hg/HgO) obtained at different SOC

System	State of charge (%)			
	97.5	95	90	80
Fe	−981	−980	−979	−984
Fe + 1.8wt.%Ag	−980	−975	−978	−980
Fe + 7.4wt.%Cu	−973	−975	−975	−976
Fe + 1.17wt.%Pb	−951	−968	−976	−980
Fe + 0.82wt.%Hg	−991	−991	−988	−980
Fe + 10.9wt.%S	−990	−991	−991	−992

have the opposite effect. Since the discharge was carried out at constant current, the shift from E_M to E'_M, towards a more noble potential, is due to oxidation of $Fe(OH)_2$ to FeOOH.

Additions of silver, copper and lead favour the oxidation of $Fe(OH)_2$ while mercury and sulphur retard it. Sulphur modifies the structure of anodic $Fe(OH)_2$-film by its diffusion, and film growth is thereby hindered. FeS appears to be more stable than $Fe(OH)_2$ [19] as the standard potential of Fe/FeS is −0.97 V *versus* NHE compared with −0.887 V for Fe/$Fe(OH)_2$.

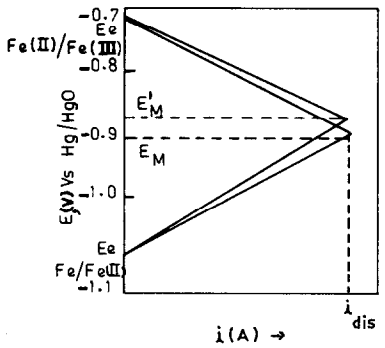

Fig. 5. Schematic mixed potential diagram.

Conclusions

(i) Several additives to the porous iron electrode increased its discharge capacity at the $Fe(OH)_2$ potential in comparison with a pure iron electrode.

(ii) The product $i\sqrt{t}$ was shown not to be constant for porous iron electrodes with, and without, additives.

(iii) Electrochemically impregnated silver, copper, and lead promoted the onset of FeOOH formation. Mercury and sulphur retarded FeOOH formation, so making them more beneficial as additives to the iron electrode in nickel–iron cells.

References

1 L. Ojefors, *Electrochim. Acta, 21* (1976) 302.
2 P. R. Vassie and A. C. C. Tseung, *Electrochim. Acta, 21* (1976) 263.
3 G. Paruthimal Kalaignan, V. S. Muralidharan and K. I. Vasu, *J. Appl. Electrochem., 17* (1987) 1083.
4 G. Paruthimal Kalaignan, V. S. Muralidharan and K. I. Vasu, *Trans. SAEST, 22* (1987) 67.
5 G. Paruthimal Kalaignan, V. S. Muralidharan and K. I. Vasu, *Bull. Electrochem. Soc., 4* (1988) 551.
6 G. Paruthimal Kalaignan, V. S. Muralidharan and K. I. Vasu, *Proc. Annu. Tech. Meeting (Electrochem. Soc. India), Bangalore, July 1985*, p. 32.
7 K. Micka and Z. Zabransky, *J. Power Sources, 19* (1987) 315.
8 N. Jayalakshmi and V. S. Muralidharan, *Br. Corros. J.*, in press.
9 J. Cerny and K. Micka, *J. Power Sources, 25* (1989) 111.
10 K. Vijayamohan, A. K. Shukla and S. Sathyanarayana, *J. Power Sources, 21* (1987) 53.
11 K. I. Vasu, V. S. Muralidharan, M. Ramakrishnan, G. Paruthimal Kalaignan and N. Jayalakshmi, *J. Power Sources, 28* (1989) 409.
12 V. S. Muralidharan and M. Veerashanmugamani, *J. Appl. Electrochem., 15* (1985) 675.

13 J. S. Newman and C. W. Tobias, *J. Electrochem. Soc., 109* (1962) 1183.
14 D. D. Mcdonald, *Transient Techniques in Electrochemistry*, Plenum Press, NY, 1977.
15 A. Hussam and G. Gunaratra, *Anal. Chem., 60* (1988) 503.
16 J. Hindea, J. Augustynski and R. Monnier, *Electrochim. Acta, 21* (1976) 459.
17 H. J. S. Sand, *Philos. Mag., 1* (1901) 45.
18 D. T. Sawyer and J. L. Roberts, *Experimental Electrochemistry for Chemists*, Wiley-Interscience, NY, 1974, p. 402.
19 W. M. Latimer, *Oxidation Potentials*, Prentice-Hall, Englewood Cliffs, NJ, 1961.